Stability of clusters in the second–order Kuramoto model on random graphs

Georgi S. Medvedev*

Mathew S. Mizuhara[†]

September 10, 2020

Abstract

The Kuramoto model of coupled phase oscillators with inertia on Erdős-Rényi graphs is analyzed in this work. For a system with intrinsic frequencies sampled from a bimodal distribution we identify a variety of two cluster patterns and study their stability. To this end, we decompose the description of the cluster dynamics into two systems: one governing the (macro) dynamics of the centers of mass of the two clusters and the second governing the (micro) dynamics of individual oscillators inside each cluster. The former is a low-dimensional ODE whereas the latter is a system of two coupled Vlasov PDEs. Stability of the cluster dynamics depends on the stability of the low-dimensional group motion and on coherence of the oscillators in each group. We show that the loss of coherence in one of the clusters leads to the loss of stability of a two-cluster state and to formation of chimera states. The analysis of this paper can be generalized to cover states with more than two clusters and to coupled systems on W-random graphs. Our results apply to a model of a power grid with fluctuating sources.

1 Introduction

Understanding principles underlying collective behavior in large networks of interacting dynamical systems is an important problem with applications ranging from neuronal networks to power grids. Many dynamical models on networks have been proposed to this effect. The Kuramoto model (KM) of coupled phase oscillators has had a widespread success due to its analytical simplicity and universality of the dynamical mechanisms that it helped to reveal. It describes the evolution of interconnected phase oscillators $u_{n,i}: \mathbb{R}^+ \to \mathbb{R}/2\pi\mathbb{Z}$ having intrinsic frequencies $\omega_{n,i}$:

$$\dot{u}_{n,i} = \omega_{n,i} + K n^{-1} \sum_{j=1}^{n} a_{n,ij} \sin(u_{n,j} - u_{n,i} + \alpha), \quad i \in [n] := \{1, 2, \dots, n\}.$$
(1.1) [KM]

The sum on the right-hand side models the interactions between the oscillators, $\alpha \in [0, 2\pi)$ determines the type of interactions (attractive vs repulsive), and K is the strength of coupling. The spatial structure of

^{*}Department of Mathematics, Drexel University, medvedev@drexel.edu

Department of Mathematics and Statistics, The College of New Jersey, mizuharm@tcnj.edu

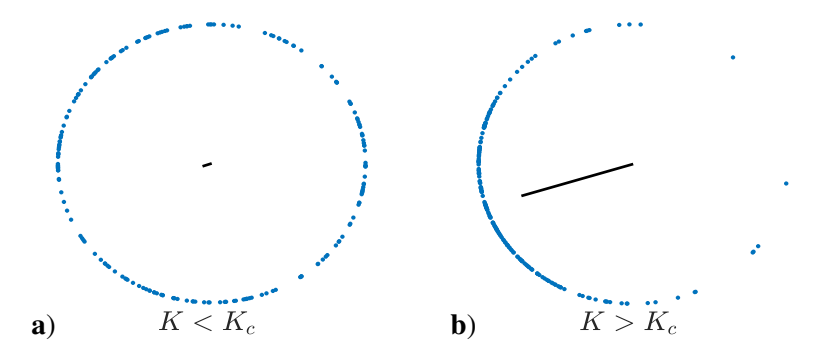


Fig. 1: The distribution of the oscillators in the phase space is shown for **a**) $K < K_c$ and for **b**) $K > K_c$. The complex order parameter is plotted as a black arrow. It points to the center of mass of the coherence buildup.

interconnections is encoded in the adjacency matrix $(a_{n,ij})$. The KM plays an important role in the theory of synchronization. We mention two major contributions that are especially relevant to the present study. First, it reveals a universal mechanism for the transition to synchronization in systems of coupled oscillators with random intrinsic frequencies. The analysis of the KM shows that there is a critical value of the coupling strength K_c separating the incoherent (mixing) dynamics (Fig. 1a) from synchronization (Fig. 1b) [?, ?, ?]. Second, studies of the KM led to the discovery of chimera states, patterns combining regions of coherent and incoherent dynamics [?, ?, ?].

Having reviewed the classical KM, we now turn to its generalization that is the main focus of this paper:

$$\ddot{u}_{n,i} + \gamma \dot{u}_{n,i} = \omega_{n,i} + K n^{-1} \sum_{i=1}^{n} a_{n,ij} \sin(u_{n,j} - u_{n,i} + \alpha), \quad i \in [n].$$
(1.2) 2KMa

The main new additions here are the second-order terms. The other parameters are the damping constant $\gamma>0$ and the random torques $\omega_{n,i}$, which we keep referring to as intrinsic frequencies to emphasize the parallels with the classical KM (1.1). The system of equations (1.2) can be viewed a model of coupled pendula. Systems of equations like (1.2) are widely used for modeling power networks [?, ?]. The inclusion of the second order terms makes the dynamics substantially more complex [?, ?, ?, ?]. In particular, the second order model is known for its capacity to generate a rich variety of coherent clusters [?, ?]. Clusters exist for different types of connectivity and different probability distributions of intrinsic frequencies. We experimented with uniform, Gaussian, and certain multimodal distributions and used all-to-all and random Erdős-Rényi (ER) connectivity. In each case, we saw an abundance of clusters (Fig. 2). Furthermore, we often found multiple cluster states coexisting for the same values of parameters (Fig. 3). Determining stability of clusters is a challenging problem. For the second order KM with identical oscillators it has been studied in [?], where the problem was reduced to the analysis of the damped pendulum equation. For the model with random intrinsic frequencies and random network topologies, numerical results related to stability of clusters can be found in [?, ?, ?]. Analytically this problem has not been studied before.

The main contribution of this paper is the general framework for studying stability of clusters in the second order KM with random intrinsic frequencies and ER random connectivity. We show that in the model with random parameters, stability of clusters is a multiscale problem. At the macroscopic level,

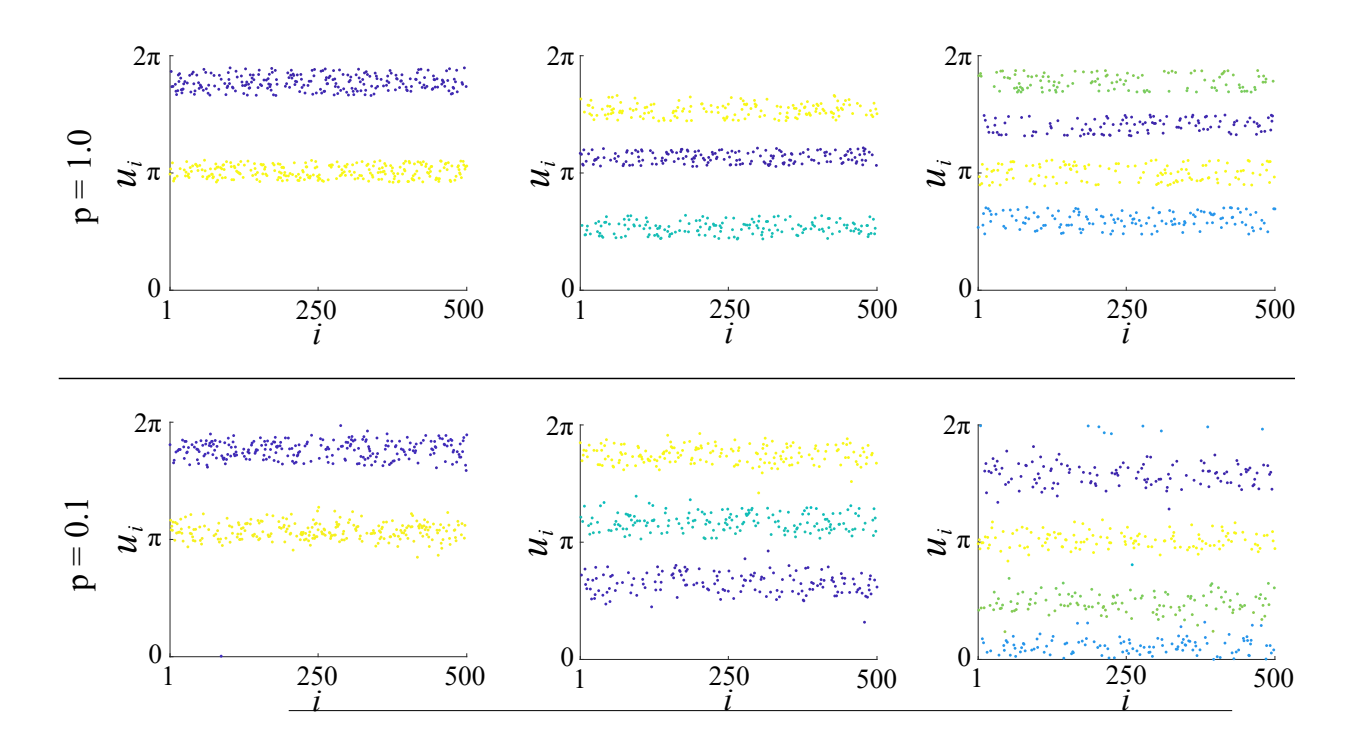


Fig. 2: The snapshots of coexisting distinct stable clusters in (1.2). The intrinsic frequencies are chosen uniformly from [-2,2]. The values of other parameters are K=3 and $\gamma=0.1$. The plots in the top line are made for the model on complete graphs and those in the bottom line on an ER graph with p=0.1. Oscillators are color coded by instantaneous velocity to reveal clustering. By choosing carefully initial conditions for the two models, one can generate 2-,3-,4- and other cluster states.

clusters have nontrivial (deterministic) dynamics. It has already been identified in the analysis of the KM with identical oscillators [?]. On the other hand: at a microscopic level, the formation of clusters requires a mechanism by which the oscillators within a cluster stay coherent, i.e., synchronization within a cluster. The second problem is intrinsically stochastic. To our knowledge, it has not been analyzed in the context of stability of clusters before. Thus, in addition to synchronization, the stability of clusters depends on the stability of the macroscopic group motion.

In the following we restrict to two-cluster states and assume a bimodal distribution of intrinsic frequencies. These assumptions are made to simplify the presentation. The same approach can be used for studying patterns with three and more groups of coherent oscillators. Likewise, the multimodality of the intrinsic frequency distribution is not necessary for cluster formation. The same mechanism is responsible for the formation of clusters when intrinsic frequencies are distributed uniformly (see Fig. 2). However, in this case additional care is needed to identify the clusters analytically. We do not address this issue in this paper. Furthermore, the same formalism applies to the KM on other random graphs [?]. We develop a general framework for studying clusters in large systems of coupled phase oscillators with randomly distributed parameters. As in [?], we write down a low-dimensional system describing the macroscopic (group) dynamics of clusters. Further, we derive a system of kinetic PDEs characterizing the stochastic dynamics of fluctuations with each cluster. The PDE for each cluster incorporates the information about the group motion as well as the fluctuations in other clusters. The low-dimensional equation for the group dynamics and the system of PDEs for fluctuations together contain all information determining the stability of clusters. The former system can be further reduced to the equation of damped pendulum and analyzed using standard methods of the qualitative theory of ordinary differential equations [?]. On the other hand, the analysis of the two coupled Vlasov equations is a hard problem, which we do not pursue in its general form. Instead, we focus on parameter regimes when the two PDEs decouple, which simplifies the analysis.

The stability analysis in these parameter regimes suggests a scenario for the loss of stability of a two-cluster state due to the loss of coherence in one of the clusters. Specifically, we show that decoupling of the system of Vlasov equations results in the fluctuations in one cluster being practically independent from the fluctuations in the other cluster. In contrast to the stability of clusters in the KM with identical oscillators in [?] or the loss of stability of solitary states in [?], the underlying bifurcation is the bifurcation of the steady state of the system of Vlasov PDEs not of the damped pendulum equation, i.e., this is an infinite-dimensional phenomenon. By controlling the fluctuations in one of the clusters we can make it incoherent, while keeping the other cluster coherent. Interestingly, this provides a new scenario of the loss of stability of a two-cluster state leading to the creation of chimera states.

The emerging chimera states differ from the previously reported ones in several respects. They do not lie close to the border between the regions of the attractive and repulsive coupling like the chimera states in the classical KM (cf. [?]). They do not depend on the block structure of the coupling (adjacency) matrix, as chimera states in [?, ?], or external noise, as chimera states in [?]. Unlike solitary states in [?], they do not rely on the existence of clusters with equal velocities. The velocities in the incoherent clusters of chimera states shown in Figs. 9, 10, and 11 are distributed over an interval.

The following paragraph still feels a bit out of place.

The coexistence of coherence and incoherence in homogeneous networks of coupled oscillators has been the most intriguing feature of chimera states since their discovery in [?]. For large systems, the most com-

prehensive explanation for such coexistence is based on the Ott-Antonsen Ansatz [?], i.e., it applies to a family of special solutions of the KM. The existence of the weak chimera states as defined in [?] is difficult to verify in large systems with random parameters. At the same time, numerous modeling and experimental studies clearly demonstrate that the coexistence of coherence and incoherence in coupled system is a universal phenomenon. In this paper, we analytically showed the existence of two-cluster states having distinct statistical properties. The distribution of the fluctuations in one cluster can be controlled independently from the distribution in the other cluster. This provides a new mechanism for spatiotemporal patterns with regions with distinct statistical properties and explains formation of chimera states shown in Figs. 8, 9, 10, and 11.

The outline of the paper is as follows. In Section 2, we develop a macro-micro decomposition of the cluster dynamics into a low dimensional (group) motion of the centers of mass of two clusters and the system of equations governing the fluctuations in each group. For the latter system, we derive a system of two Vlasov PDEs describing the probability densities for the fluctuations in the limit as the number of oscillators in each cluster tends to infinity. The macro-micro decomposition of the cluster dynamics is the main tool and the main contribution of this paper. In Section 3, we review the key facts about the dynamics of a damped pendulum [?] that will be needed below. In Section 4, we turn to the analysis of fluctuations. We identify two parameter regimes when the two Vlasov equations decouple and the coherence in each cluster can be analyzed separately. We use linear stability analysis of the incoherent state in the KM with inertia [?] to locate the critical values for the loss of coherence in each cluster. Then we identify parameters where oscillators in one cluster lose coherence, while the oscillators in the other cluster remain synchronized. This leads to formation of chimera states. We illustrate this scenario with numerical experiments. Numerics are consistent with the theoretical predictions. We conclude with a brief discussion of the main results.

2 The macro-micro decomposition

sec.macro

sec.model

2.1 The model

For simplicity, we restrict our study to a two-cluster case¹. To this end, we assume a bimodal distribution for $\omega_{n,i}$'s. Specifically, we assume that there are two groups of oscillators u_1, u_2, \ldots, u_m and $u_{m+1}, u_{m+1}, \ldots, u_{m+l}, n = m+l$. The intrinsic frequencies assigned to the oscillators in the first and second groups are taken from probability distributions with densities $\tilde{g}_1(\omega)$ and $\tilde{g}_2(\omega)$ respectively. Denote the first two central moments by

$$\bar{\omega}_1 = \int \omega \tilde{g}_1(\omega) d\omega, \ \bar{\omega}_2 = \int \omega \tilde{g}_2(\omega) d\omega, \ \sigma_1^2 = \int (\omega - \bar{\omega}_1)^2 \tilde{g}_1(\omega) d\omega, \ \sigma_2^2 = \int (\omega - \bar{\omega}_1)^2 \tilde{g}_1(\omega) d\omega. \ (2.1) \quad \boxed{\texttt{moments}}$$

We assume

$$\delta = \bar{\omega}_2 - \bar{\omega}_1 > 0, \quad 0 < \sigma_1^2, \sigma_2^2 \ll \delta, \tag{2.2}$$

assume-mom

and $g_{1,2}(y) = \tilde{g}_{1,2}(\bar{\omega}_{1,2} + y)$ are even unimodal functions. Further, we assume that the initial positions and velocities for each cluster $\{u_{n,k}(0)\}_{k=1}^m$, $\{\dot{u}_{n,k}(0)\}_{k=1}^m$, $\{u_{n,m+k}(0)\}_{k=1}^l$, $\{\dot{u}_{n,m+k}(0)\}_{k=1}^l$, are sequences of independent identically distributed (each sequence has its own distribution in general) random variables, which satisfy assumptions of the Strong Law of Large Numbers.

¹It is easy to generalize the equations determining stability of d-cluster stattes for $d \ge 2$, but the analysis of this system is already challenging for d = 2.

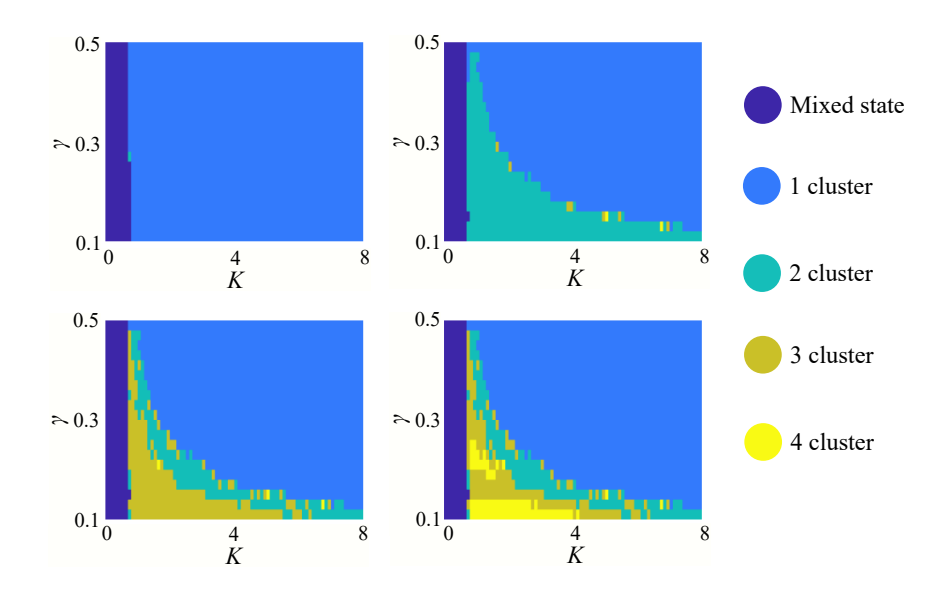


Fig. 3: Regions of existence of stable d-cluster states shown for for $d=1, 1 \le d \le 2, 1 \le d \le 3$ and $1 \le d \le 4$ superimposed on each other. The diagrams show a substantial region in the parameter space with coexisting stable 1-, 2-, 3-, and 4-cluster states. The frequencies are sampled from the uniform distribution on [-0.5, 0.5] and coupling is all-to-all.

In addition, we assume that the underlying network has sparse (should this say dense?) ER connectivity:

$$\mathbb{P}\left(a_{n,ij}=1\right) = p_n,\tag{2.3}$$

where (p_n) is a positive nonincreasing sequence that is either $p_n \equiv p \in [0, 1]$ or $p_n \searrow 0$ such that $p_n n \to \infty$ as $n \to \infty$. In the latter case, we obtain a sequence of sparse ER graphs of unbounded degree. Thus, below we study the following system of ODEs²:

$$\ddot{u}_{n,i} + \gamma \dot{u}_{n,i} = \omega_{n,i} + K(p_n n)^{-1} \sum_{j=1}^{n} a_{n,ij} \sin(u_{n,j} - u_{n,i} + \alpha), \quad i \in [n].$$
 (2.4)

The analysis of this can be easily generalized to a more general W-random graph model (cf. [?]). We restrict to the ER case to keep the notation simple.

2.2 The group dynamics

In this and the following subsections, we decompose the dynamics of clusters into two systems: one governing the macroscopic dynamics of individual clusters and the second governing the microscopic dynamics of individual particles inside each cluster. The former is a system of low dimensional ODEs and the latter is a system of PDEs of Vlasov type.

²See [?] for more details on the KM on sparse graphs.

The Ansatz to be introduced below relies on the average position of oscillators within a cluster. To define the latter, we have to resolve an ambiguity of the mean of S-valued variables. Consider, for instance, the average value of $\pi/2$ and $3\pi/2$ as elements of S. Both 0 and π may be viewed as the mean of these two numbers from geometric viewpoint. To avoid this ambiguity, it is convenient to work with lifts $\hat{u}_{n,i}(t)$, of $u_{n,i}(t)$, $i \in [n]$, to \mathbb{R} . Specifically, let $\hat{u}_{n,i}: \mathbb{R} \to \mathbb{R}$ stand for a continuous function such that

$$(\hat{u}_{n,i}(t) - u_{n,i}(t)) = 0 \pmod{2\pi} \ t \ge 0.$$

There are infinitely many 'copies' of $\hat{u}_{n,i}(t)$. We assume that for each oscillator one can choose an appropriate copy such that the Ansatz below holds. By abuse of notation we will drop the hats in the notation of $\hat{u}_{n,i}(t)$.

Denote

$$U_{n,1} = m^{-1} \sum_{k=1}^{m} u_{n,k}, \ U_{n,2} = l^{-1} \sum_{k=1}^{l} u_{n,m+k},$$
 (2.5) anz

where

$$v_{n,i} = u_{n,i} - U_{n,1}, \qquad i \in [m],$$

 $v_{n,m+j} = u_{n,m+j} - U_{n,2}, \qquad j \in [l].$ (2.6) def-v

We assume that the dynamics in each cluster are (predominantly) coherent:

$$\max_{i \in [n]} |v_i| \le \varepsilon \ll 1. \tag{2.7}$$

Adding up the first m equations in (1.1) and dividing by m, we have

$$\ddot{U}_{n,1} + \gamma \dot{U}_{n,1} = \bar{\omega}_{n,1} + \frac{K}{mnp_n} \sum_{i=1}^{m} \sum_{j=1}^{m} a_{n,ij} \sin(v_{n,j} - v_{n,i} + \alpha)
+ \frac{K}{mnp_n} \sum_{i=1}^{m} \sum_{j=1}^{l} a_{n,ij} \sin(U_{n,2} - U_{n,1} + [v_{n,m+j} - v_{n,i}] + \alpha).$$
(2.8) U1

Rewrite the last sum on the right-hand side of (2.8) as

$$\sum_{i=1}^{m} \sum_{j=1}^{l} a_{n,ij} \sin (U_{n,2} - U_{n,1} - \alpha + v_{n,m+j} - v_{n,i}) = \sum_{i=1}^{m} \sum_{j=1}^{l} a_{n,ij} \left\{ \sin (U_{n,2} - U_{n,1} + \alpha) \cos (v_{n,m+j} - v_{n,i}) + \cos (U_{n,2} - U_{n,1} - \alpha) \sin (v_{n,m+j} - v_{n,i}) \right\}$$

$$+ \cos (U_{n,2} - U_{n,1} - \alpha) \sin (v_{n,m+j} - v_{n,i}) \right\}$$
(2.9) Sin-cos

and note

$$\cos(v_{n,m+j} - v_{n,i}) = 1 - o(1), \sin(v_{n,m+j} - v_{n,i}) = o(1).$$

After plugging (2.9) into (2.8) and separating O(1) terms, we obtain the following IVP for the dynamics

of the first cluster

$$\ddot{U}_{n,1} + \gamma \dot{U}_{n,1} = \bar{\omega}_{n,1} + \frac{Kl}{n} \sin(U_{n,2} - U_{n,1} + \alpha), \qquad (2.10)$$

$$U_{n,1}(0) = m^{-1} \sum_{k=1}^{m} u_{n,k}(0), \qquad (2.11)$$

$$\dot{U}_{n,1}(0) = m^{-1} \sum_{k=1}^{m} \dot{u}_{n,k}(0)$$
(2.12)

where we also used

$$m^{-1}\sum_{i=1}a_{n,ij}=p_n+o(1)$$
 with high probability.

We will assume that $mn^{-1} \to \chi \in (0,1)$, and so $ln^{-1} \to 1-\chi$ as $n \to \infty$. By the Law of Large Numbers, $\bar{\omega}_{n,1} \to \bar{\omega}_1$, $m^{-1} \sum_{k=1}^m u_{n,k}(0) \to \bar{u}_1$. Likewise, $m^{-1} \sum_{k=1}^m \dot{u}_{n,k}(0) \to \bar{u}_1$ as $n \to \infty$. Thus, for $n \gg 1$, (2.10), (2.11) is approximated by

$$\ddot{U}_1 + \gamma \dot{U}_1 = \bar{\omega}_1 + K(1 - \chi) \sin(U_2 - U_1 + \alpha), \qquad (2.13)$$

$$U_1(0) = \bar{u}_1, (2.14)$$

$$\dot{U}_1(0) = \dot{\bar{u}}_1. \tag{2.15}$$

Similarly, we obtain the system approximating the dynamics of the second cluster

$$\ddot{U}_2 + \gamma \dot{U}_2 = \bar{\omega}_2 + K \chi \sin(U_1 - U_2 + \alpha), \qquad (2.16)$$

$$U_2(0) = \bar{u}_2, (2.17)$$

$$\dot{U}_2(0) = \dot{\bar{u}}_2. \tag{2.18}$$

sec.fluc

2.3 The fluctuations

Next, we turn to the analysis of the fluctuations $v_{n,i}$, $i \in [n]$. After plugging in (2.5) into the equation for the oscillator $i \in [m]$ and using (2.8), we have

$$\begin{split} \ddot{v}_{n,i} + \gamma \dot{v}_{n,i} &= \xi_{n,i} + \frac{K}{np_n} \sum_{j=1}^m a_{n,ij} \sin \left(v_{n,j} - v_{n,i} + \alpha \right) \\ &+ \frac{K}{np_n} \sum_{j=1}^l a_{n,ij} \left\{ \sin \left(U_{n,2} - U_{n,1} + \alpha \right) \left[\cos \left(v_{n,m+j} - v_{n,i} \right) - 1 \right] \right. \\ &+ \left. \cos \left(U_{n,2} - U_{n,1} + \alpha \right) \sin \left(v_{n,m+j} - v_{n,i} \right) \right\} \\ &- \frac{K}{mnp_n} \sum_{i=1}^m \sum_{j=1}^l a_{n,ij} \sin \left(U_{n,2} - U_{n,1} \right) \left[\cos \left(v_{n,m+j} - v_{n,i} \right) - 1 \right] \\ &- \frac{K}{mnp_n} \sum_{i=1}^m \sum_{j=1}^l a_{n,ij} \cos \left(U_{n,2} - U_{n,1} + \alpha \right) \sin \left(v_{n,m+j} - v_{n,i} \right) \ i \in [m], \end{split}$$

where $\xi_{n,i} = \omega_{n,i} - \bar{\omega}_{n,1}$. For large $n, \xi_{n,i}, i \in [n]$ are approximated by independent identically distributed (IID) random variables (RVs) $\xi_i, i \in [n]$, having probability density g_1 .

Since $|v_{n,i}| = o(1)$, terms

$$1 - \cos(v_{n,m+j} - v_{n,i}) = 2\sin\left(\frac{v_{n,m+j} - v_{n,i}}{2}\right)^2, \ j \in [l],$$

are of higher order and can be dropped. Further, we approximate $U_{n,1}$ and $U_{n,2}$ by U_1 and U_2 respectively. Thus, (2.19) simplifies to

$$\ddot{v}_{n,i} + \gamma \dot{v}_{n,i} = \xi_i + \frac{K}{np_n} \sum_{j=1}^m a_{n,ij} \sin(v_{n,j} - v_{n,i} + \alpha)$$

$$+ \frac{K}{np_n} \sum_{j=1}^l a_{n,ij} \cos(U_2 - U_1 + \alpha) \sin(v_{n,m+j} - v_{n,i})$$

$$- \frac{K}{mnp_n} \sum_{i=1}^m \sum_{j=1}^l a_{n,ij} \cos(U_2 - U_1 + \alpha) \sin(v_{n,m+j} - v_{n,i}) \quad i \in [m],$$
(2.20) Corr-la

Next, we show that

$$\frac{1}{mnp_n} \sum_{i=1}^{m} \sum_{j=1}^{l} a_{n,ij} \sin(v_{n,m+j} - v_{n,i}) = o(1).$$
 (2.21) [double-sum

By the Taylor's formula and triangle inequality, we have

$$\left| \frac{1}{mnp_n} \sum_{i=1}^{m} \sum_{j=1}^{l} a_{n,ij} \sin \left(v_{n,m+j} - v_{n,i} \right) \right| \leq \left| \frac{1}{mnp_n} \sum_{i=1}^{m} \sum_{j=1}^{l} a_{n,ij} \left(v_{n,m+j} - v_{n,i} \right) \right| + \left| \frac{1}{6mnp_n} \sum_{i=1}^{m} \sum_{j=1}^{l} a_{n,ij} \left(v_{m+j} - v_i \right)^3 \right|$$

$$= \left| \frac{1}{mn} \sum_{i=1}^{m} \sum_{j=1}^{l} \frac{a_{n,ij}}{p_n} \left(v_{n,m+j} - v_{n,i} \right) \right| + O(\epsilon^3).$$
(2.22) \text{ taylor-exp}

Further, since

$$\sum_{j=1}^{m} v_{n,j} = \sum_{j=1}^{l} v_{n,m+j} = 0,$$

the sum in first term on the right hand side of (2.22) can be written as

$$\frac{1}{mn} \sum_{i=1}^{m} \sum_{j=1}^{l} \frac{a_{n,ij}}{p_n} \left(v_{n,m+j} - v_{n,i} \right) = \frac{1}{mn} \sum_{i=1}^{m} \sum_{j=1}^{l} \xi_{n,ij} \left(v_{n,m+j} - v_{n,i} \right),$$

where $\xi_{n,ij} = \frac{a_{n,ij}}{p_n} - 1$ are independent zero–mean random variables. If we assume that all v_i 's are bounded almost surely, then the application of Bernstein inequality yields that for any $0 < \varepsilon < 1/2$

$$\frac{1}{mn} \sum_{i=1}^{m} \sum_{j=1}^{l} \frac{a_{n,ij}}{p_n} \left(v_{n,m+j} - v_{n,i} \right) = \frac{1}{mn} \sum_{i=1}^{m} \sum_{j=1}^{l} \xi_{n,ij} \left(v_{n,m+j} - v_{n,i} \right) = O(n^{-\frac{1}{2} + \varepsilon})$$
 (2.23) [first-term]

with high probability. The combination of (2.22) and (2.23) yields (2.21).

Thus, we arrive at the following equation

$$\ddot{v}_{n,i} + \gamma \dot{v}_{n,i} = \xi_i^{(1)} + \frac{K}{np_n} \sum_{j=1}^m a_{n,ij} \sin(v_{n,j} - v_{n,i} + \alpha)$$

$$+ \frac{K}{np_n} c(t) \sum_{j=1}^l a_{n,ij} \sin(v_{n,m+j} - v_{n,i}), i \in [m],$$
(2.24) [corr-1-fin]

where

$$c(t) = \cos\left(U_2 - U_1 + \alpha\right). \tag{2.25}$$

The terms on the first line of (2.24) constitute the KM for one cluster. The sum on the second line yields the contribution from the other cluster.

Similarly, we derive the system of equations of fluctuations in the second cluster

$$\ddot{v}_{n,m+i} + \gamma \dot{v}_{n,m+i} = \xi_i^{(2)} + \frac{K}{n} \sum_{j=1}^{l} \sin(v_{n,m+j} - v_{n,m+i} + \alpha) + \frac{K}{n} c(t) \sum_{j=1}^{m} \sin(v_{n,j} - v_{n,m+i} + \alpha), \quad i \in [l],$$
(2.26) Corr-2

where $\xi_i^{(2)}$, $i \in [l]$ are iid RVs whose distribution has density g_2 .

To analyze large systems (2.19) and (2.26) we use the mean field limit approximation. To this end, suppose $f_1(t, u, v, \omega)$ and $f_2(t, u, v, \omega)$ stand for the probability densities of the oscillators in the first and second clusters respectively. Then

$$\partial_t f_1 + \partial_u (v f_1) + \partial_v (V_1 f) = 0 \tag{2.27}$$

where

$$V_{1}(u, v, \omega) := \omega - \gamma v + K\chi \int_{\mathbb{S} \times \mathbb{R} \times \mathbb{R}} \sin(\phi - u + \alpha) f_{1}(t, \phi, \psi, \lambda) g_{1}(\lambda) d\phi d\psi d\lambda$$

$$+ K(1 - \chi)c(t) \int_{\mathbb{S} \times \mathbb{R} \times \mathbb{R}} \sin(\phi - u + \alpha) f_{2}(t, \phi, \psi, \lambda) g_{2}(\lambda) d\phi d\psi d\lambda, \quad \chi = mn^{-1}.$$

$$(2.28) \quad \boxed{\forall -1}$$

Similarly,

$$\partial_t f_2 + \partial_u \left(v f_2 \right) + \partial_v \left(V_2 f_2 \right) = 0 \tag{2.29}$$

where

$$V_{2}(u, v, \omega) := \omega - \gamma v + K(1 - \chi) \int_{\mathbb{S} \times \mathbb{R} \times \mathbb{R}} \sin(\phi - u + \alpha) f_{2}(t, \phi, \psi, \omega) g_{2}(\lambda) d\phi d\psi d\lambda$$

$$+ K \chi c(t) \int_{\mathbb{S} \times \mathbb{R} \times \mathbb{R}} \sin(\phi - u + \alpha) f_{1}(t, \phi, \psi, \omega) g_{1}(\lambda) d\phi d\psi d\lambda.$$

$$(2.30) \quad \boxed{\forall -2}$$

The mathematical justification for using Vlasov equation to study the dynamics of the KM with all-to-all coupling in the large n limit was provided by Lancellotti [?]. It is based on the classical results on Vlasov equation [?]. For the KM on convergent sequences of dense graphs the use of the Vlasov equation was justified in [?, ?]. To extend this justification to sparse graphs with unbounded degree like the Erdős-Rényi graphs used in this work, it sufficient to combine these results with Theorem 4.1 in [?] (see [?] for a related analysis of the α -Hamiltonian mean field model). Finally, the results for the first-order KM in these papers apply to the higher dimensional models after trivial modifications.

In the numerical experiments below, we are going to use the following order parameters computed for each cluster:

$$R_1(t) = \frac{1}{m} \sum_{i=1}^m e^{iu_{n,j}}, \quad R_2(t) = \frac{1}{l} \sum_{i=1}^l e^{iu_{n,j}}.$$
 (2.31) [order]

The modulus of $R_1(R_2)$ measures the degree of coherence in cluster 1 (2): with values close to 0 corresponding to a high degree of mixing and those close to 1 corresponding to a high degree of coherence. For simulations we compute the average value of the modulus of the order parameter over a time interval, after a long initial transient period. We denote these values $|R_{1,\infty}|$ and $|R_{2,\infty}|$, respectively.

3 The damped pendulum equation

sec.group

To continue we need to understand the group dynamics (2.13), (2.16). To this end, we change variables to

$$X = U_2 - U_1$$
, $S = (1 - \chi)^{-1}U_1 + \chi^{-1}U_2$, (3.1) New-var

and rewrite (2.13), (2.16) as

$$\ddot{X} + \gamma \dot{X} = \delta - K \left(\chi \sin(X - \alpha) + (1 - \chi) \sin(X + \alpha) \right), \quad \delta := \bar{\omega}_2 - \bar{\omega}_1 > 0, \tag{3.2}$$

$$\ddot{S} + \gamma \dot{S} = \delta_0, \quad \delta_0 := (1 - \chi)^{-1} \bar{\omega}_1 + \chi^{-1} \bar{\omega}_2.$$
 (3.3)

In the remainder of this section, we restrict to $\chi = 1/2$, as this is the value used in all our experiments. For the treatment of (3.2) for other values of χ , we refer the interested reader to [?]. For $\chi = 1/2$, we have

$$\ddot{X} + \gamma \dot{X} = \delta - K \cos(\alpha) \sin(X). \tag{3.4}$$

Equation (3.2) is the damped pendulum equation with constant torque. Qualitative dynamics of (3.2) can be understood using phase plane analysis [?]. To this end, rewrite (3.2) as

$$\dot{X} = Y, \tag{3.5}$$

$$\dot{Y} = \delta - \gamma Y - K \cos \alpha \sin X. \tag{3.6}$$

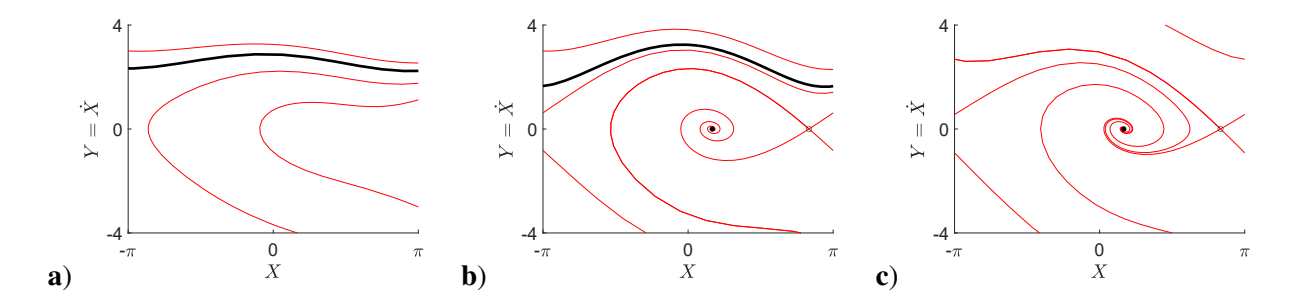


Fig. 4: Phase plane plots illustrating three structurally stable regimes for the damped pendulum. a) The black trajectory corresponds to the stable periodic orbit (when viewed on the cylinder). b) Two fixed points appear in a saddle–node bifurcation. Thus, we have a stable focus coexisting with a stable periodic orbit. c) The periodic orbit disappears in a homoclinic bifurcation. The stable focus remains the only attractor.

f.pplane

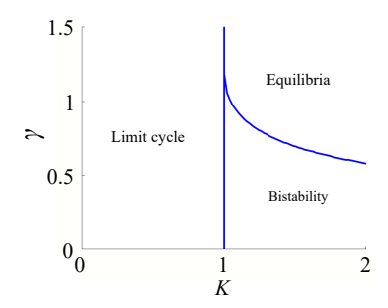


Fig. 5: Bifurcation diagram illustrating three qualitatively distinct regimes in the damped pendulum model (3.7), (3.8).

f.bifD

Note that by rescaling variables and parameters $Y := \delta^{-1/2}Y$, $\gamma := \delta^{-1/2}\gamma$, and $K := \delta^{-1/2}K\cos\alpha$, and changing time we can scale out δ :

$$\dot{X} = Y,$$

$$\dot{Y} = 1 - \gamma Y - K \sin X.$$
(3.7)
$$(3.8)$$

$$Y = 1 - \gamma Y - K \sin X. \tag{3.8}$$

Thus, without loss of generality one can set $\delta = 1$.

We summarize the phase plane analysis of the damped pendulum equation (3.7), (3.8) and refer the interested reader to [?] for more details. First, it is easy to see that for K > 1 the system has a pair of equilibria:

$$(X_e, 0) \text{ and } (\pi - X_e, 0), X_e = \arcsin K^{-1}.$$
 (3.9) equil

equilib

The former is a stable focus while the latter is a saddle. They collide in a saddle-node bifurcation at K=1and disappear for K < 1. Further, for K < 1 the Poincaré-Bendixson theorem implies existence of a limit cycle, which must be stable as the divergence of the vector field is equal to $-\gamma < 0$ (Fig. 4a). The limit cycle persists for $K \geq 1$ provided that $0 < \gamma \leq \gamma_{hom}(K)$ (Fig. 4b). At $\gamma = \gamma_{hom}(K)$, the system undegoes a homoclinic bifurcation (Fig. 4c). Thus, there are three parameter regimes with qualitatively distinct dynamics shown in Fig. 5: In (I) and (II) the attractor is a limit cycle and stable focus respectively. In (III) both the limit cycle and the stable focus coexist.

ec.chimera

4 The loss of coherence and chimera states

4.1 The overview of synchronization in the second-order KM

In this section, we describe a mechanism for the loss of stability of a two-cluster state due to the loss of synchronization in one of the clusters. We show that this leads to the creation of chimera states. To this end, it is instructive first to review synchronization in a single all—to—all coupled population of second—order phase oscillators:

$$\ddot{u}_{n,i} + \gamma \dot{u}_{n,i} = \xi_i + K n^{-1} \sum_{i=1}^n \sin(u_{n,i} - u_{n,i}), \quad i \in [n], \tag{4.1}$$

where ξ_i are IID RVs taken from a probability distribution with density g. Throughout this discussion, we assume that g is a unimodal even function. If the initial conditions are drawn from the continuous probability distribution then the distribution of the phase of oscillators in the extended phase space $\mathbb{S} \times \mathbb{R} \times \mathbb{R}$ remains absolutely continuous with respect to the Lebesgue measure for every t>0. The density $f(t,u,v,\omega)$ satisfies the following Vlasov equation (cf. [?])

$$\partial_t f + \partial_u (vf) + \partial_v (Vf) = 0, \tag{4.2}$$

where

$$V := \omega - \gamma v + K \int_{\mathbb{S} \times \mathbb{R} \times \mathbb{R}} \sin(\phi - u) f(t, \phi, \psi, \omega) g(\lambda) d\phi d\psi d\lambda. \tag{4.3}$$

The Vlasov equation (4.2), (4.3) has a steady state solution:

$$ar{f}(u,v) = rac{\delta_{\omega/\gamma}(v)}{2\pi},$$
 (4.4) MFsteady

where $\delta_{\omega/\gamma}(v) = \delta(v-\gamma/\omega)$ is Dirac delta function centered at γ/ω . It describes the configuration when phases are distributed uniformly over the unit circle, while velocities are localized around ω/γ . This is an incoherent or mixing state. Linear stability analysis of (4.2) about \bar{f} shows that there is a critical value $K_c>0$ such that the mixing state is stable for $K\in[0,K_c]$ and and is unstable for $K>K_c$. For $\alpha=0$ the value of K_c is known explicitly [?]

$$K_c = 2\left(\pi g(0) - \int_{\mathbb{R}} \frac{g(\omega)}{\gamma^2 + \left(\frac{\omega}{\gamma}\right)^2} d\omega\right)^{-1}.$$
 (4.5) [KC]

Equation (4.5) is not essential for the main results of this paper. It is in a good agreement with our numerical results and is included to better illustrate the loss of coherence within clusters in the numerical experiments below.

4.2 The loss of coherence within a cluster

The macro-micro decomposition yields the following picture of cluster dynamics in the second order KM. The macroscopic evolution of two subpopulations is described by the damped pendulum equation (3.7),

(3.8). On the other hand the fluctuations in the two subpopulations are described by the system of two coupled Vlasov equations (2.27), (2.28) and (2.29), (2.30). The coupling between (2.27), (2.28) and (2.29), (2.30) is modulated by the group dynamics through c(t) (see (2.25)). For stability of a two-cluster configuration, we need a stable solution of the pendulum equation. In addition, we need fluctuations in both groups to remain small. There are two qualitatively distinct stable states of the equation for the group motion:

- A) a stable fixed point resulting in the phase locked (stationary) clusters (Fig. 4 b,c),
- **B**) a stable limit cycle resulting in two clusters moving in opposite directions³ (Fig. 4 **a,b**).

The corresponding clusters are shown in Fig. 6. For each of this cases, we show that one can desynchronize the oscillators in one cluster without affecting the oscillators in the other cluster.

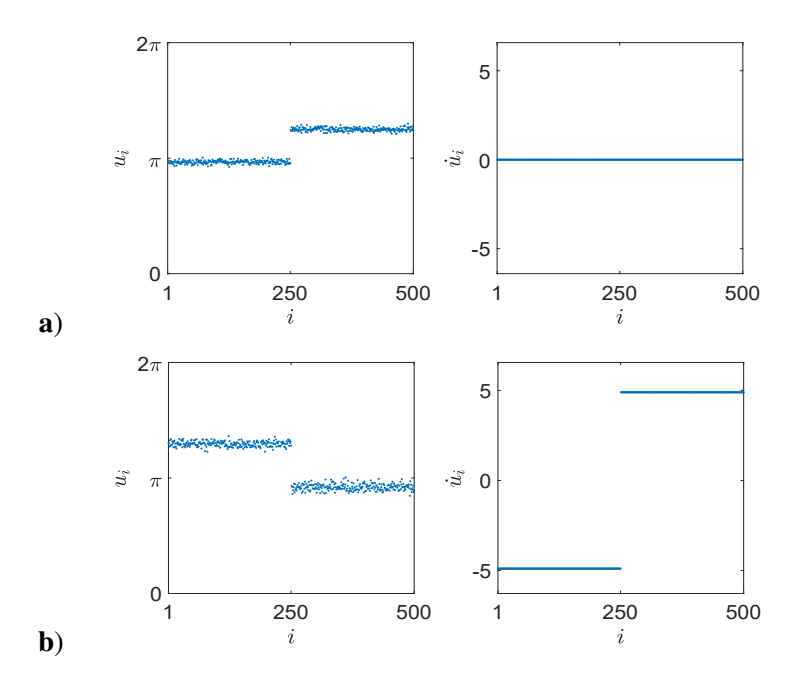


Fig. 6: Two qualitatively distinct types of clusters: **a**) stationary and **b**) moving. The corresponding stable states of the pendulum equation (3.7), (3.8) are a stable fixed point and a limit cycle respectively. The values of parameters used for both plots are $\gamma = 0.1$ and ω chosen from $\mathcal{N}(\pm 0.5, 0.05)$.

f.5

We consider stationary clusters first. Recall the damped pendulum equation (3.7), (3.8) governing the group dynamics. For K > 1, it has a pair of fixed points (Fig. 5), one of which is stable (cf. (3.9)). We suppose that the group dynamics is driven by the stable equilibrium. We will locate parameter regimes where the fluctuations in the two clusters become practically independent. Then we demonstrate that the fluctuations in each cluster can be controlled separately. In particular, we will desynchronize one cluster, while keeping the other one coherent.

³We maintain $\bar{\omega}_1 < 0 < \bar{\omega}_2$ in all numerical experiments.

We start with the case of $\alpha = 0$. When the system (3.7), (3.8) is at the stable equilibrium (cf. (3.9)),

$$U_2 - U_1 = \arcsin\left(\frac{1}{K\cos(\alpha)}\right),\tag{4.6}$$

so $c(t) = \frac{\sqrt{K^2 - 1}}{K}$. Thus, for K just above 1,

$$0 < K - 1 \ll 1, (4.7)$$

we have $c(t)\approx 0$. In this regime, the two Vlasov equations describing the coherence in the two clusters are practically decoupled. Thus, we can treat each cluster as a separate population of oscillators and compute the critical values of the coupling strength using (4.5) for each cluster separately. Next we choose the variances of the distributions of intrinsic frequencies σ_1^2 and σ_2^2 such that

$$K_c(\sigma_1^2) < K < K_c(\sigma_2^2).$$

Then for a given value of K the mixing state is stable for the first cluster, while it is unstable for the second cluster. As a result, we get a chimera state with the oscillators in the first cluster distributed uniformly while the oscillators in the second cluster remain synchronized (see Fig. 7).

The same idea can be used to generate chimera states for an arbitrary value of K by changing α . In this case, $c(t) = \cos(U_2 - U_1 + \alpha)$ from (4.6) we have

$$c(t) = \cos\left(\arcsin\left(\frac{1}{K\cos(\alpha)}\right) + \alpha\right).$$

An application of the intermediate value theorem shows that there exists an $\alpha := \alpha^* \in (0, \arccos(K^{-1}))$ such that

$$\arcsin\left(\frac{1}{K\cos(\alpha^*)}\right) + \alpha^* = \frac{\pi}{2}.\tag{4.8}$$

With this choice of α , we can make $c(t) \equiv 0$ and the two Vlasov equations decouple as before. We now choose the variances $\sigma_{1,2}^2$ sufficiently small so that both clusters are coherent for a given K > 1. In particular,

$$\max\{K_c(\sigma_1^2, \alpha), K_c(\sigma_2^2, \alpha)\} < K, \tag{4.9}$$

find alpha

i.e., the incoherent state is unstable for each cluster. Note that since the Vlasov equations are uncoupled, we can compute the critical values $K_c(\sigma_1^2,\alpha)$ and $K_c(\sigma_1^2,\alpha)$ for each cluster separately. In Appendix A we show that K_c is an increasing function of σ . Thus, we can keep σ_2^2 fixed and and increase σ_1^2 so that

$$K_c(\sigma_2^2, \alpha) < K < K_c(\sigma_1^2, \alpha).$$
 (4.10) after

Now the second cluster remains coherent, while the first cluster transitions to the newly stable mixing state, thus, giving rise to a chimera state. The results of this experiment are presented in Figs. 8a and 9.

In the numerical experiments above we used the explicit expression of the stable equilibrium (3.9) to compute the value of α^* , for which the coupling coefficient c(t) vanishes (cf. (4.8)). Instead one can use the following adaptive scheme to guide the system into the regime where c(t) becomes very small. ⁴ To this end, let us add the following differential equation for α :

$$\dot{\alpha} = \cos(U_2 - U_1 + \alpha). \tag{4.11} eg:alpha_c$$

⁴Note that we are not using the analytic equation for α^* .

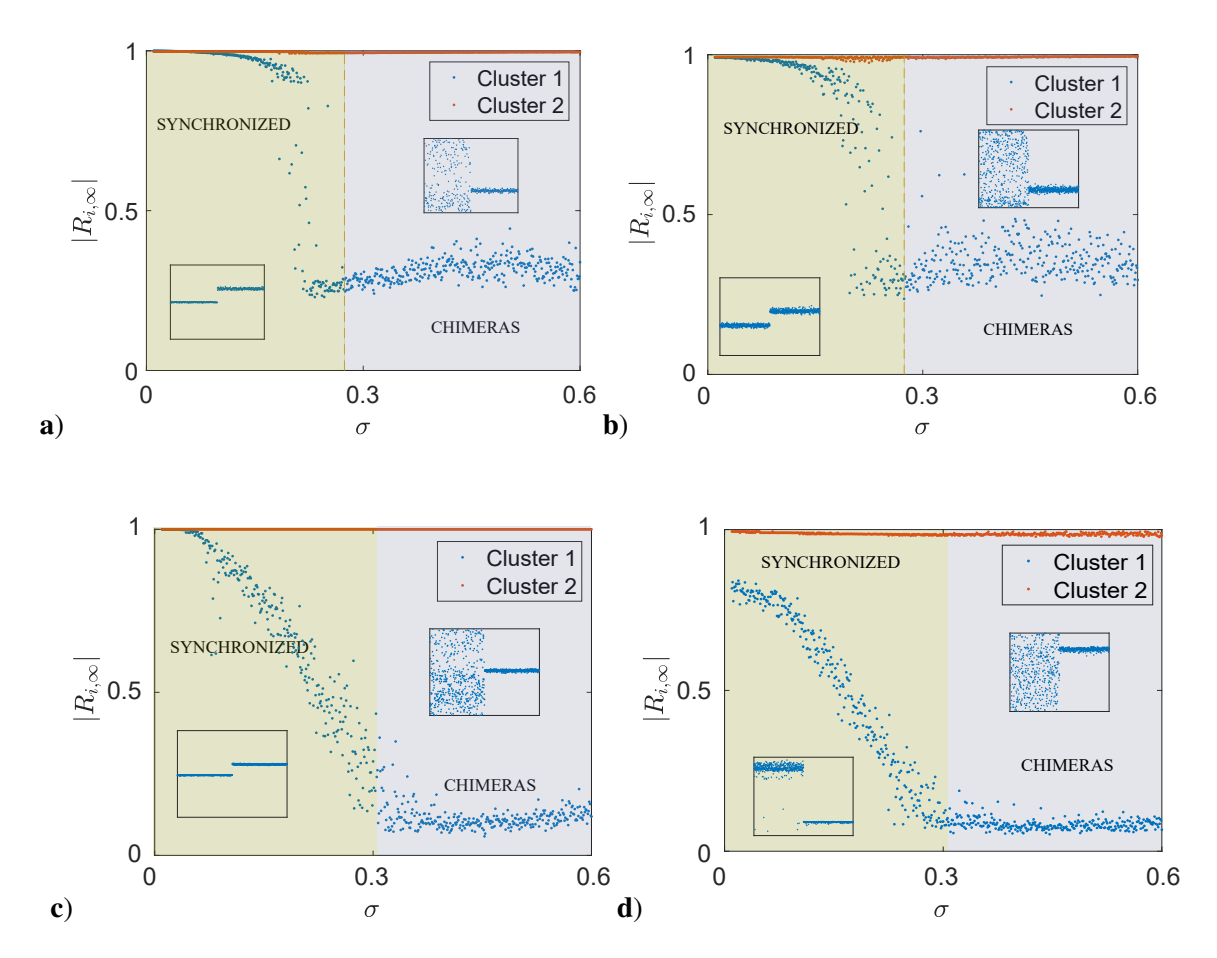


Fig. 7: For $0 < K-1 \ll 1$ the system for the group dynamics (3.7), (3.8) has a stable fixed point. When the group dynamics is driven by the stable fixed point, $c(t) \approx 0$ (see the text). For a given K, we use (4.5) to compute the critical value of the variance σ_*^2 , at which the incoherent state loses stability. Plots show the time averaged magnitude of the order parameters (2.31) after a transient period, denoted $|R_{i,\infty}|$, i=1,2. When the variance of the distribution of the intrinsic frequencies for the first cluster is increased beyond σ^* (dotted line) the first cluster desynchronizes. This results in the formation of chimera state. **a**) All-to-all coupling and **b**) ER connectivity with p=0.1. Other parameters are K=1.1 and $\gamma=1$. The same experiment was repeated for K=2, $\gamma=0.5$, and $\alpha=0.7854$. The results are shown for **c**) all-to-all coupling and **d**) ER graph with p=0.5.

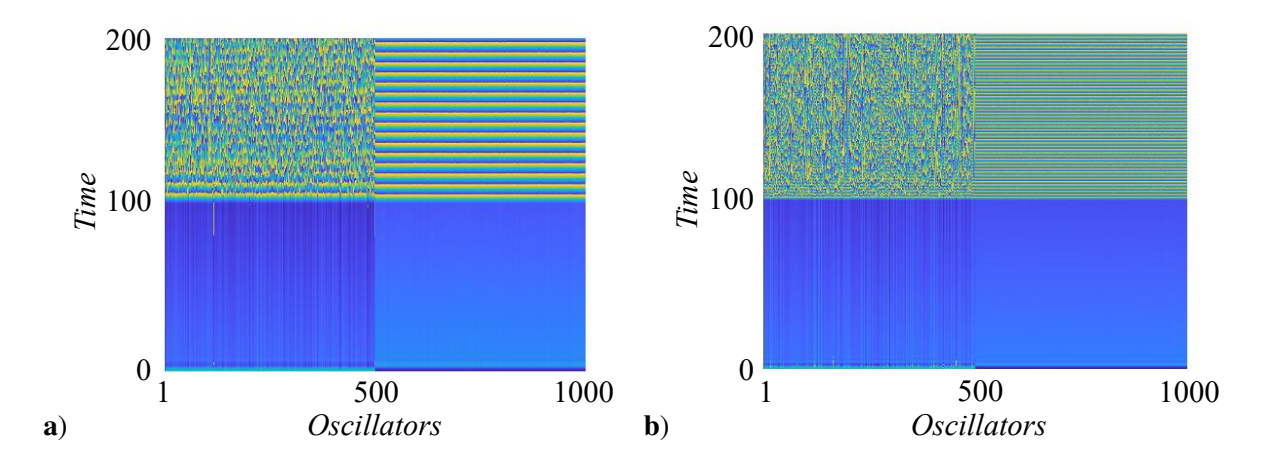


Fig. 8: Plots show the evolution of oscillators (horizontal axis) over time (vertical axis) with phase indicated by color. Before t=100, we fix $\alpha=0$. a) At t=100 instantaneously let $\alpha=\alpha^*$ (the solution of (4.8)). See also Figure 9. b) At t=100 let α evolve by (4.11). See also Figure 10. In both cases the first cluster desynchronizes resulting in the emergence of a chimera state. We take all-to-all connectivity, and parameters are $\gamma=1$, K=5, and frequencies are chosen from N(-0.5,0.9) and N(0.5,0.05).

f.chimera

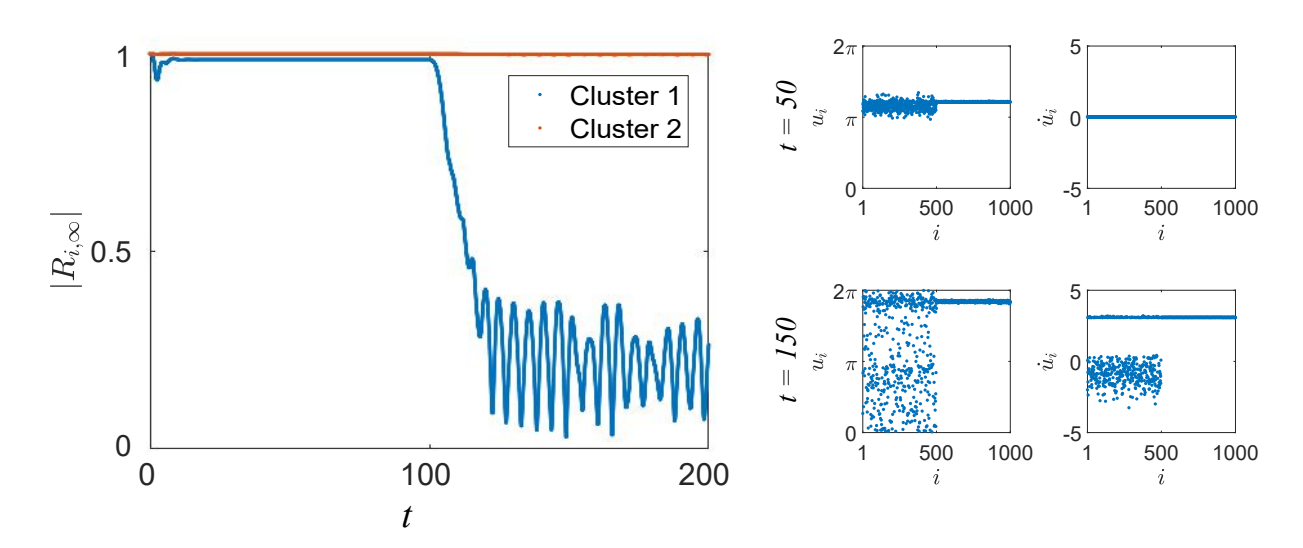


Fig. 9: Starting the simulation with $\alpha=0$ fixed, we observe phase-locked solutions (top right shows solution snapshot at time t=50). At t=100 we instantaneously let $\alpha=\alpha^*$ (the solution of (4.8)) and observe the emergence of a chimera state (bottom right shows solution snapshot at t=150). The left panel shows the order parameter of each cluster over time. Here we take all-to-all connectivity, $\gamma=1, K=5$, and frequencies are chosen from $\mathcal{N}(-0.5,0.9)$ and $\mathcal{N}(0.5,0.05)$.

f.9

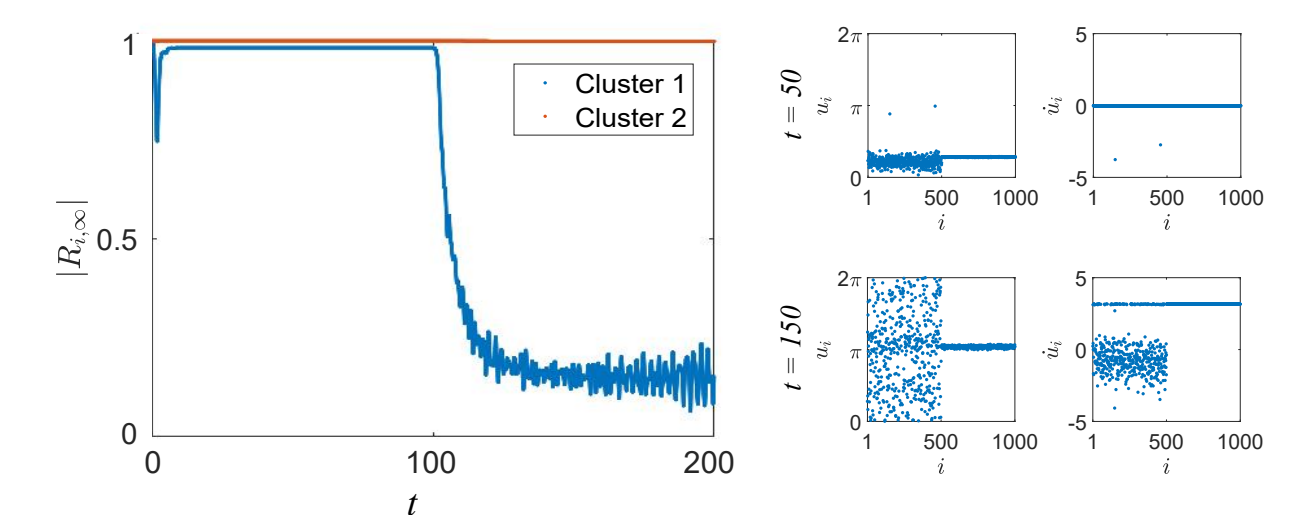


Fig. 10: Starting the simulation with $\alpha=0$ fixed, we observe phase-locked solutions (top right shows solution snapshot at time t=50). At t=100 we let α evolve by (4.11) and see the emergence of a chimera state (bottom right shows solution snapshot at t=150). The left panel shows the order parameter of each cluster over time. Here we take all-to-all connectivity, $\gamma=1, K=5$, and frequencies are chosen from $\mathcal{N}(-0.5,0.9)$ and $\mathcal{N}(0.5,0.05)$.

f.dotalpha

The right-hand side of (4.11) depends on the average values of u computed for the first and the second cluster

$$U_1 = m^{-1} \sum_{k=1}^{m} u_k, \ U_2 = l^{-1} \sum_{k=1}^{l} u_k.$$
 (4.12)

Note that at any fixed point of (4.11), $c(t) = \cos(U_2 - U_1 + \alpha)$ is automatically zero. Thus, after short transients we expect that the evolution of α forces c(t) to become very small and to stay small for all future times. We verified this scenario numerically in the experiment illustrated in Figs. 8b and 10.

Finally, we turn to the case when the group dynamics are driven by a limit cycle. In this case, it is easy to find the values of parameters for which the velocity $\dot{U}_2 - \dot{U}_1$ along the limit cycle is sufficiently large and approximately constant (see Fig. 4a). Then $c(t) \approx \cos(\omega t + \tau)$ for some $\omega \gg 1$ and phase shift τ (Fig. 11a). Note that the average value of c is 0 and as before, i.e., we effectively have uncoupled equations for the fluctuations in the two clusters. Using this observation, we can construct numerical examples illustrating the loss of stability of two-cluster states leading to chimera states (Fig. 11).

5 Generalizations

s.final

We end this paper with a few remarks on possible generalizations and extensions of the analysis of this paper.

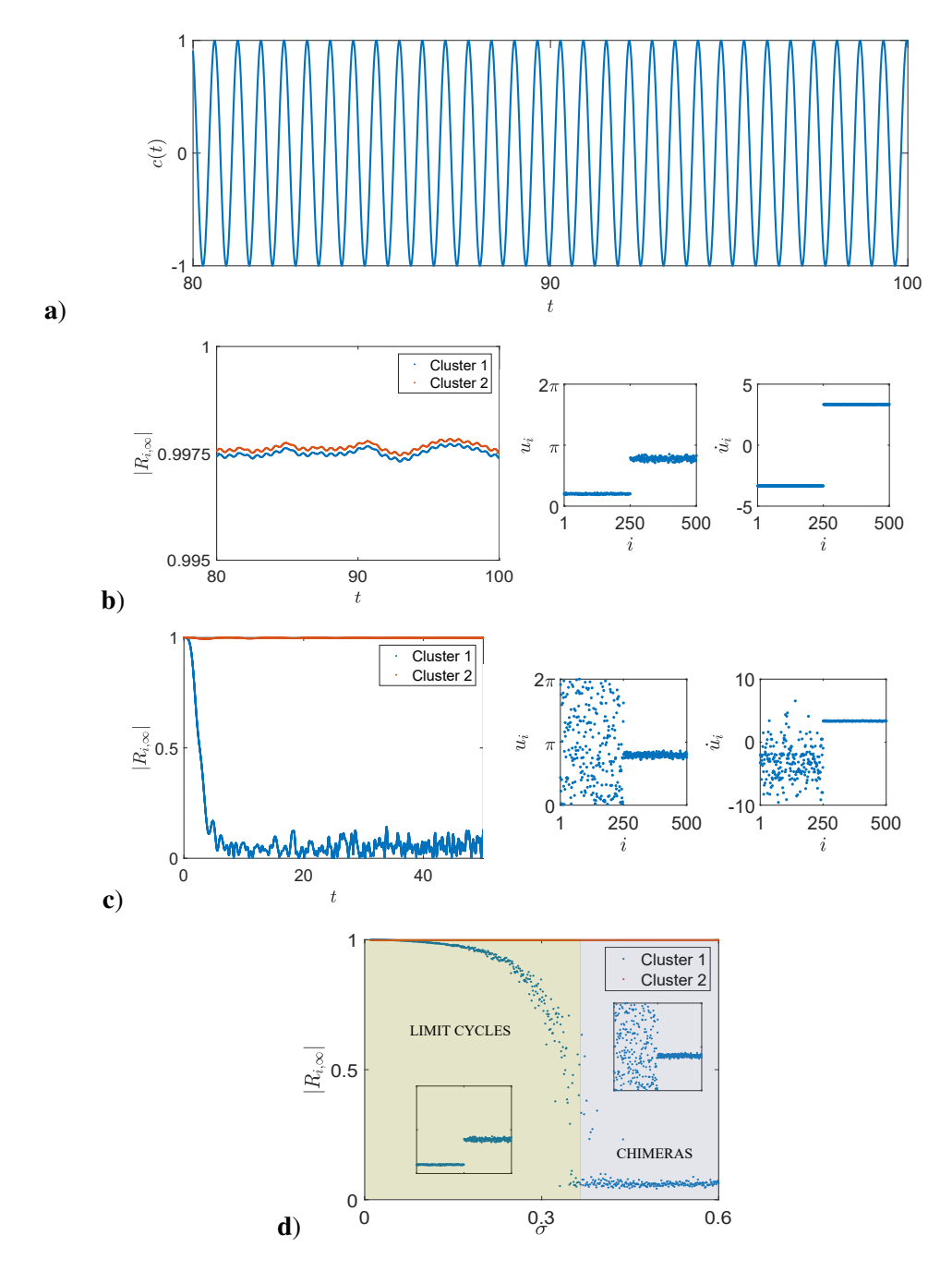


Fig. 11: Taking parameters $\gamma=0.1, K=1.5$ with all-to-all connectivity, we generate two coherent clusters moving in opposite directions rapidly. a) The coupling coefficient c(t) oscillates rapidly around 0. b) Taking frequencies chosen from $\mathcal{N}(\pm 0.5, 0.05)$ both clusters remain synchronized. The order parameters for both clusters remain close to 1 for all times. c) Next taking frequencies of the first cluster from $\mathcal{N}(-0.5, 0.5)$, cluster 1 desynchronizes, while cluster 2 remains synchronous. d) The order parameters of each cluster when frequencies of the first cluster are taken from $\mathcal{N}(-0.5, \sigma)$, with representative snapshots inset.

5.1 Clusters in the first-order KM

The analysis of clusters in the KM with inertia in the main part of the paper applies verbatim to the first order KM (1.1). Below, we outline the main steps and comment on the differences in the analyses of the two models.

We continue to assume that the frequencies are sampled from the bimodal distribution (cf. Section 2.1). For simplicity, let $\chi = 1/2$ and $\alpha \in (-\pi/2, \pi/2)$. The equations for the group dynamics become

$$\dot{U}_1 = \bar{\omega}_1 + K \sin(U_2 - U_1 + \alpha),\tag{5.1}$$

$$\dot{U}_2 = \bar{\omega}_2 + K \sin(U_1 - U_2 + \alpha),$$
 (5.2)

and the equation for $X = U_2 - U_1$ takes the following form

$$\dot{X} = \delta - K\cos(\alpha)\sin(X).$$
 (5.3) [1KM-pend

As before we assume that $\delta=\bar{\omega}_2-\bar{\omega}_1>0$. For $|\delta/(K\cos\alpha)|<1$, (5.3) has a single stable fixed point $\bar{X}=\arcsin{(\delta/(K\cos\alpha))}$. For $|\delta/(K\cos\alpha)|>1$, $\dot{X}>0$. The former regime corresponds to a stationary phase–locked clusters, while the latter results in moving clusters. No multistability is possible in the first–order model.

The system of two Vlasov equations describing the fluctuations for the first–order system is derived in exactly the same way as in § 2.3. Further, the two Vlasov equations can decoupled by either setting $\alpha = \alpha^*$ (cf. (4.8)) or by evolving α with the help of an additional differential equation (4.11). Thus, the fluctuations in the two clusters can be made independent and can be controlled separately exactly in the same way as before (see Figure 13).

5.2 Sparse graphs

The analysis of this paper covers the KM on sparse graphs of unbounded degree (cf. (2.4)). The numerical simulations presented in this paper were done with the KM on dense Erdős–Rényi graphs. We expect that all effects described in this paper continue to hold for the KM on sparse graphs provided that n is sufficiently large. Figure 14 shows the results of numerical experiments in Figure 7 but on sparse Erdős–Rényi graphs with $p_n = n^{-1/10}$. The results shown in these figures agree well.

5.3 Multiple clusters and general graphs

The analysis of this paper can be used to study patterns with d>2 clusters. Indeed, the micro-macro decomposition of Section 2 extends to d>2 clusters in a sraightforward way. Clearly, for d>2 it does not seem possible to describe all attractors. Nontheless, we were able to identify some stable steady states and periodic orbits for d=3,4 (not presented in this paper). Formally, the stability conditions for d-clusters remain the same, albeit one has to deal with a system of d Vlasov equations in general. One can be decouple them as before provided multiple phase lag parameters $\alpha_1,\alpha_2,\ldots,\alpha_{d-1}$ are available.

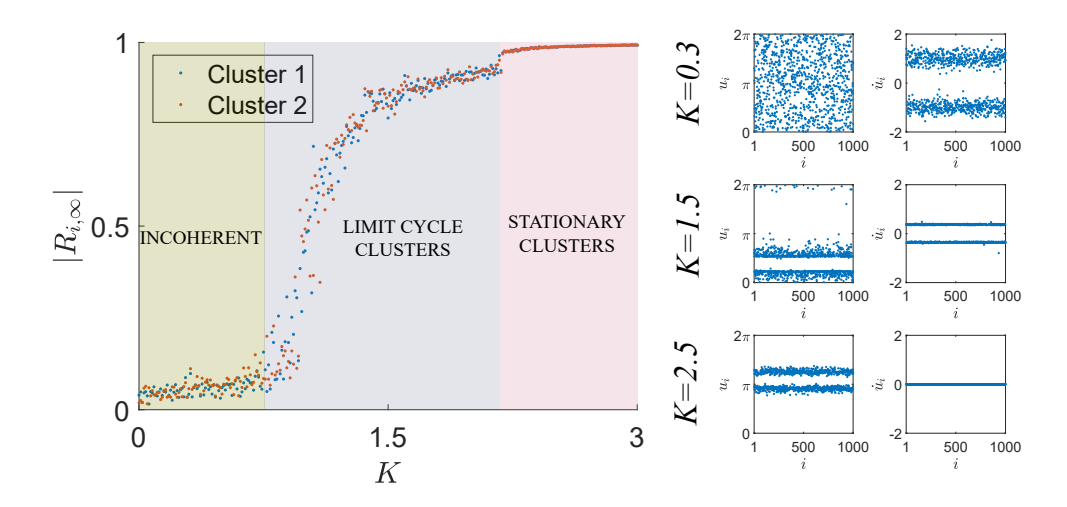


Fig. 12: Bifurcations in the first—order Kuramoto model with all-to-all coupling and intrinsic frequencies sampled from symmetric bimodal distribution. The parameters are chosen such that the two—cluster bifurcating from the incoherent state is not stationary (see text for discussion). One further sees a second bifurcation, which results in the stationary two—cluster. Interestingly, the first bifurcation is the bifurcation of the incoherent state, as a steady state of the system of two Vlasov equations, while the second one can traced to the transformations of the vector field for the group dynamics (cf. (5.3)).

f.1KM-bif

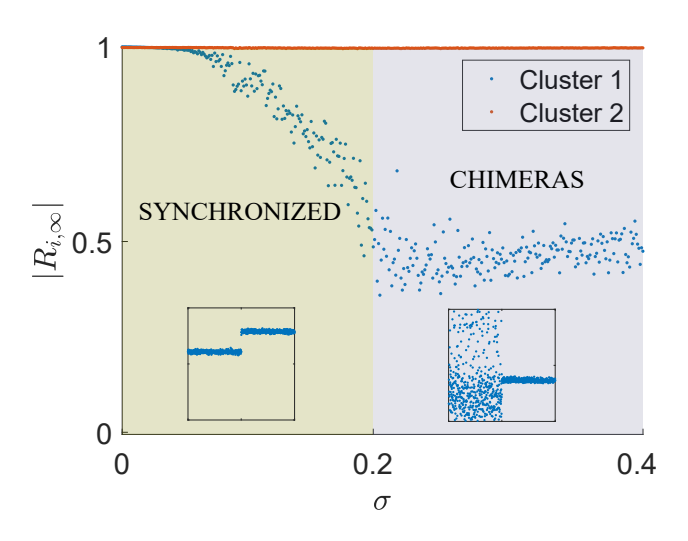


Fig. 13: The loss of coherence in one cluster in the first–order model (1.1) with all-to-all coupling. We start with a stable two–cluster ($K=1.1,\,\mu_{1,2}=\pm0.5,\,\sigma_{1,2}=0.05$). Then we decouple the fluctuations by setting $\alpha=\alpha^*$. Finally, keeping σ_2 fixed, we vary σ_1 .

f.1KM-loss

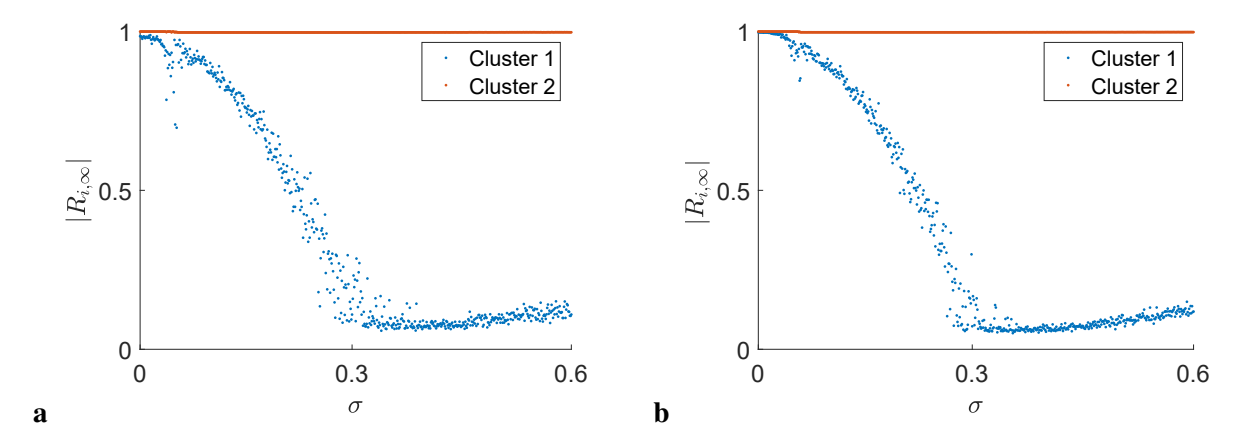


Fig. 14: The numerical results in **a** and **b** correspond to the experimental results in Figure 7 **c** and **d**, but on sparse Erdős–Rényi graphs with $p_n = n^{-1/10}$ with **a**) n = 1000 oscillators and **b**) n = 2000 oscillators.

f.sparse

Furthermore, as we remarked earlier, our approach naturally extends to systems on more general random graphs (cf. [?]). The studies of the classical KM of coupled phase oscillators made substantial contribution to our understanding of synchronization in coupled systems [?]. The second order KM holds an equal potential for the formation of clusters in large coupled dynamical systems.

Acknowledgements. This work was supported in part by NSF grants DMS 1715161 and 2009233 (to GSM). Numerical simulations were completed using the high performance computing cluster (ELSA) at the School of Science, The College of New Jersey. Funding of ELSA is provided in part by National Science Foundation OAC-1828163. MSM was additionally supported by a Support of Scholarly Activities Grant at The College of New Jersey.

A K_c is an increasing function of σ

sec.a

Suppose q zero mean Gaussian density with standard deviation σ

$$g(s) = \frac{1}{\sigma\sqrt{2\pi}} \exp\left(-\frac{s^2}{2\sigma^2}\right). \tag{A.1}$$

By plugging (A.1) into (4.5) we have

$$K_c(\sigma) = 2\sqrt{2\pi}\sigma \left(\pi - \int_{\mathbb{R}} \frac{\exp\left(-\frac{s^2}{2\sigma^2}\right)}{\gamma^2 + (s/\gamma)^2} ds\right)^{-1},$$

which can be further rewritten as

$$K_c(\sigma) = \frac{2\sqrt{2}\sigma}{\sqrt{\pi}} \left(1 - \exp\left(\frac{\gamma^4}{2\sigma^2}\right) \operatorname{Erfc}\left(\frac{\gamma^2}{\sigma\sqrt{2}}\right) \right)^{-1}, \tag{A.2} \quad \text{kc_gaussia}$$

where $\operatorname{Erfc}(x) = 1 - \frac{2}{\sqrt{\pi}} \int_0^x e^{-s^2} ds$ is the function.

Lemma A.1. K_c in (A.2) is an increasing function of $\sigma > 0$.

Proof. Let $A=\exp\left(\frac{\gamma^4}{2\sigma^2}\right)\mathrm{Erfc}\left(\frac{\gamma^2}{\sigma\sqrt{2}}\right)$ and note that

$$\frac{dK_c}{d\sigma} = \frac{2\sqrt{2}}{\sqrt{\pi}} \left((1-A) + \sigma(1-A)^{-2} \frac{dA}{d\sigma} \right).$$

Below we show that A<1 and $\frac{dA}{d\sigma}>0$ for all $\sigma>0$. Assume first that $\sigma<\gamma^2$. Then, using the well known bound

$$\operatorname{Erfc}(z) < \frac{\exp(-z^2)}{\sqrt{\pi}z},$$
 (A.3) $\operatorname{erfc_est1}$

it follows that $A < \frac{\sqrt{2}\sigma}{\sqrt{\pi}\gamma^2} < 1$.

Next consider when $\sigma \geq \gamma^2$. Since the Taylor series expansion of $\operatorname{Erfc}(z)$ is an alternating series

$$\operatorname{Erfc}(z) = 1 - \frac{2}{\sqrt{\pi}} \left(z - \frac{z^3}{3} + \frac{z^5}{10} - \dots \right),$$
 (A.4)

we have

$$\text{Erfc}(z) < 1 - \frac{2}{\sqrt{\pi}}z + \frac{2}{3\sqrt{\pi}}z^3.$$
 (A.5)

Thus,

$$A < \exp\left(\frac{\gamma^4}{2\sigma^2}\right) \left(1 - \frac{\sqrt{2}}{\sqrt{\pi}} \cdot \frac{\gamma^2}{\sigma} + \frac{1}{3\sqrt{2\pi}} \cdot \frac{\gamma^6}{\sigma^3}\right). \tag{A.6}$$

In this case we have

$$A < e^{1/2} \left(1 - \frac{\sqrt{2}}{\sqrt{\pi}} + \frac{1}{3\sqrt{2\pi}} \right) < 1.$$
 (A.7) [A.7]

Finally, we show that $\frac{dA}{d\sigma}>0$. Indeed, by direct calculation,

$$\frac{dA}{d\sigma} = \frac{\sqrt{2}\gamma^2}{\sqrt{\pi}\sigma^2} - \frac{\gamma^4}{\sigma^3} \exp\left(\frac{\gamma^4}{2\sigma^2}\right) \operatorname{Erfc}\left(\frac{\gamma^2}{\sigma\sqrt{2}}\right).$$

Again use (A.3) to see that

$$\frac{dA}{d\sigma} > \frac{\sqrt{2}\gamma^2}{\sqrt{\pi}\sigma^2} - \frac{\gamma^4}{\sigma^3} \cdot \frac{\sqrt{2}\sigma}{\sqrt{\pi}\gamma^2} = 0. \tag{A.8}$$

References